united nations
educational, scientific
and cultural
organization

international atomic
energy agency

the
abdus salam
international centre for theoretical physics

H4.SMR/1330-1

" Sixth Workshop on Non-Linear Dynamics and Earthquake Prediction"

15 - 27 October 2001

A Boolean Delay Equation Model of Colliding Cascades
Part I: Multiple Seismic Regimes

I. Zaliapin, V. Keilis-Borok

International Institute of Earthquake Prediction Theory
and Mathematical Geophysics, Russian Academy of Sciences
Moscow, Russia
University of California at Los Angeles
Los Angeles, California, U.S.A.

M. Ghil
Department of Atmospheric Sciences and
Institute of Geophysics and Planetary Physics
University of California at Los Angeles
Los Angeles, California, U.S.A.

A Boolean Delay Equation Model of Colliding Cascades. Part I: Multiple Seismic Regimes

Ilya Zaliapin [*],

Vladimir Keilis-Borok[†], and

Michael Ghil[‡]

[*]International Institute of Earthquake Prediction Theory and Mathematical Geophysics, Russian Academy of Science, Moscow, Russia, and Institute of Geophysics and Planetary Physics, University of California at Los Angeles, Los Angeles, California, E-mail: zal@ess.ucla.edu

[†]International Institute of Earthquake Prediction Theory and Mathematical Geophysics, Russian Academy of Science, Moscow, Russia, and Institute of Geophysics and Planetary Physics and Department of Earth and Space Sciences, University of California at Los Angeles, Los Angeles, California, E-mail: vkb@ess.ucla.edu

[‡]Department of Atmospheric Sciences and Institute of Geophysics and Planetary Physics, University of California at Los Angeles, Los Angeles, California, 90095-1565. E-mail: mghil@igpp.ucla.edu, Phone: (310) 206-0651 Fax: (310) 206-5219, corresponding author.

Abstract

We consider a prominent and poorly understood feature of hierarchical nonlinear ("complex") systems: persistent recurrence of abrupt overall changes, called here "critical transitions." Unlike studying phase transitions in statistical physics, we consider large deviations from steady state that culminate in a critical transition, rather than the steady states themselves.

Motivated by the earthquake prediction problem, we formulate a model that uses heuristic constraints taken from the dynamics of seismicity. Our conclusions, though, may apply to hierarchical systems that arise in other areas.

We use the Boolean delay equation (BDE) framework to model the dynamics of colliding cascades. The phenomenon of colliding cascades comprises interaction of direct cascades of loading and inverse cascades of failures. Using the BDE framework, we replace the elementary interactions of elements in the system by their integral effect. This effect is represented by the time delays between consecutive switching of an element's state, i. e. between unloaded vs. loaded and intact vs. failed states. In this way we bypass the necessity to reconstruct the detailed behavior of the system from complex and diverse interactions, for which our knowledge is very incomplete. This simplifies the systematic study of the model's dynamics without losing its essential features.

The present paper is the first of two on the BDE approach to modeling seismicity. Its major results are the following: (i) A model that implements the approach. (ii) Simulating three basic types of seismic regime. (iii) A study of regime switching in parameter space, depending on the rates of loading and healing.

The second paper focuses on the prediction problem. We demonstrate that the model exhibits four major types of premonitory seismicity patterns observed in nature. Their individual and collective performance in prediction is explored by error diagrams and found to be high in the model.

Keywords Cellular automata; Delay equations; Hierarchical modeling; Colliding cascades; Seismic regimes.

1 Background

1.1 Colliding cascades (CC) models

The CC models [1, 2, 3] synthesize three phenomena that play an important role in many complex systems: (i) The system has a hierarchical structure, with the smallest elements merging in turn to form larger and larger ones. (ii) The system is continuously loaded (or driven) by external sources. (iii) The elements of the system fail (break down) under the load, causing redistribution of the load and strength throughout the system. Eventually the failed elements heal, thereby ensuring the continuous operation of the system. We use in our models the ternary hierarchical structure, as shown in Fig. 1.

The load is applied at the top of the hierarchy and transferred downwards to the smallest elements, thus forming a *direct cascade of loading.* Failures are initiated at the lowest level of the hierarchy, and gradually propagate upwards, thereby forming an *inverse cascade of failures*, which is followed by *healing.* The interaction of direct and inverse cascades establishes the dynamics of the system: loading triggers the failures, while failures redistribute and release the load.

The above fundamentals allow a variety of ways to model a phenomenon of colliding cascades. The CC model first introduced by Gabrielov et al. [1] has employed a system of ordinary differential equations (ODEs) to simulate elementary interactions among elements. This system was running in continuous time; load and fatigue of each element were also continuous. The ODE version of the CC model has reproduced certain major features of seismicity, including four types of premonitory seismicity patterns. Among them is a new type of premonitory patterns — increase of the earthquake correlation range — which was found in the CC model first [2] and then in observations [4]. The study of this model led to the conclusion that further simplification was desirable to explore the colliding cascades phenomenon [1].

Closest to the present study is the second version of the CC model [3], which is based on a cellular automaton (CA) in discrete time. It has discrete state variables — load and fatigue. The CA version retains all the features of the ODE version that are essential for our study. Moreover the CA version made it easier to explore scaling properties of the system, including the scale invariance of aftershock generation.

The present version of the model goes further in its simplicity and transparent dependence of behavior on control parameters by taking advantage of the BDE framework developed by M. Ghil and associates [5, 6]. This version will be used in our study's second part [7] to explore premonitory seismicity patterns of synthetic seismicity.

The study's first part (the present paper) proceeds as follows. The remainder of the present section provides some background on BDEs and the model's heuristic constraints. The model is formulated in Sec. 2 and its multiple seismic regimes are described in Sec. 3. The physics of what determines the prevalence of one regime or another is outlined in Sec. 4 and the results are further discussed in Sect. 5.

1.2 Boolean delay equations (BDEs)

BDEs are a novel modeling language especially tailored for the mathematical formulation of conceptual models of systems that exhibit threshold behavior, multiple feedbacks and distinct time delays. Originally inspired by theoretical biology, Ghil and colleagues [5, 6, 8] recognized the potential of BDEs for modeling the multiple feedbacks between the components of the climate system. They intended BDEs as a heuristic first step on the way to understanding problems too complex to model using systems of partial differential equations at the present time. One hopes, of course, to be able to eventually write down and solve the exact equations that govern the most intricate phenomena. Still, in climate dynamics as well as in solid-earth geophysics and elsewhere in the natural sciences, much of the preliminary discourse is often conceptual [9, 10]. BDEs offer a formal mathematical language that may help bridge the gap between qualitative and quantitative reasoning.

BDEs may be classified as *semi-discrete dynamical systems*, where the variables are discrete — typically Boolean, i.e. taking the values 0 ("off") or 1 ("on") only — while time is allowed to be continuous. As such they occupy the previously "missing corner" in the rhomboid of Fig. 2, where dynamical systems are classified according to whether their time (t) and state variables (x) are continuous or discrete.

Systems in which both variables and time are continuous are called *flows* [11, 12] (upper corner in the rhomboid of Fig. 2). Vector fields, ordinary and partial differential equations (ODEs and PDEs), functional and delay-differential equations (FDEs and DDEs) and stochastic differential equations (SDEs) belong to this category. Systems with continuous variables and discrete time (middle left corner) are known as *maps* [13, 14] and include diffeomorphisms, as well as ordinary and partial difference equations (O$\triangle$Es and P$\triangle$Es). Automata (lower corner) have both discrete time and variables: cellular automata (CAs) and all Turing machines (including real-world computers) are part of this group [15, 16]. BDEs and their predecessors, kinetic and conservative logic, complete the rhomboid in the figure and occupy the remaining middle right corner.

The primary motivation that led Ghil and associates [5, 6, 8] to formulate BDEs was their desire to analyze in a more precise way the implications of descriptive conceptual models prevalent in the interpretation of paleoclimate records [17, 18, 19]. Mysak et al. [20] and Ghil and co-authors [21, 22] have also pointed out the possibility to use BDEs and similar formal models in a broader climate modeling context. Further inspiration came from advances in theoretical biology, following upon Jacob and Monod's [23] discovery of on-off interactions between genes, which had prompted the formulation of "kinetic logic" [24, 25] and Boolean regulatory networks [26]. As the study of complex systems garners increasing attention and is applied to diverse areas — from economics to the evolution of civilizations, passing through physics — related Boolean and other discrete models are being explored more and more [15, 27, 28, 29].

Our BDE model uses only integer time delays. As follows from Ghil and Mullhaupt's *"pigeon-hole" lemma* [6], all BDE systems with *rational* delays can be reduced in effect to finite CAs. Commensurability of the delays creates a partition of the time axis into segments over which state variables remain constant and whose length is an integer multiple of the delays' least common denominator. As there is only a finite number of possible assignments of two values to these segments, repetition must occur, and the only asymptotic behavior possible is eventual constancy or periodicity in time.

The model studied here has a stochastic component. Its dynamics is therefore statistically stationary or cyclo-stationary, rather than simply constant or periodic.

1.3 Heuristic constraints

In its application to seismicity, the model's hierarchical structure represents a fault network [31, 30], loading imitates the impact of tectonic forces, and failures imitate earthquakes. Heuristic constraints include the major regularities in the observed dynamics of seismicity [32, 33, 34, 35]: (i) the seismic cycle; (ii) intermittency in the seismic regime; (iii) the size distribution of earthquakes, usually called the Gutenberg-Richter relation; (iv) clustering of earthquakes in space and time; (v) long-range correlations in earthquake occurrence; and (vi) a variety of seismicity patterns premonitory to a strong earthquake [32, 35, 36, 37, 38].

2 The Model

2.1 Introduction

Lattice models of systems of interacting elements are widely applied for modeling seismicity, starting from the pioneering works of Burrige and Knopoff [39], Allegre et al. [40], Bak et al. [41] and Narkunskaya and Shnirman [42]. The state of the art is summarized in [37, 43, 44, 45]. The predictability of such systems is discussed in [44, 46, 47, 48, 49]. The present study is close in spirit to the modeling described in [40, 48, 49, 50, 51, 52, 53, 54, 55]. The theoretical background for such modeling is discussed in [34, 44, 45, 47, 56, 57, 58, 59, 60]

To model colliding cascades in the BDE framework, we replace the detailed interactions between elements in the system by their integral effects. These effects can be represented by the time delays between consecutive switching of an element's state, i. e. between unloaded vs. loaded and intact vs. failed states. In this way we hope to bypass the necessity to reconstruct the system's detailed behavior from the complex and diverse interactions [52, 53, 54, 61] that are not directly accessible to observation and measurement.

Indeed, we demonstrate here that this modeling framework simplifies the systematic study of the colliding cascades dynamics without losing its essential features.

2.2 Structure

(i) The model acts on the ternary graph of depth L shown in Fig. 1a. Each element is a parent of three children that are siblings to each other. An element is connected to and interacts with its six nearest neighbours: the parent, two siblings, and three children.

(ii) Each element possesses a certain degree of *weakness* or *fatigue*, which varies as the inverse of its strength. An element fails when its weakness exceeds a certain threshold.

(iii) The model runs in discrete time $n = 0, 1, \ldots$. At each epoch a given element may be either *intact* or *failed (broken)*, and either *loaded* or *unloaded*. The state of an element e at a moment n is defined by two Boolean functions, $s_e(n)$ and $l_e(n)$: $s_e(n) = 0$ if an element is intact and $s_e(n) = 1$ if an element is in a filed state, while $l_e(n) = 0$ if an element is unloaded and $l_e(n) = 1$ if an element is loaded.

Thus, an element may be in one of the four states defined by the 2-dimensional vector $(s_e,\ l_e)$, as depicted in Table 1. Such a 2-dimensional vector of Boolean variables has been used by Saunders and Ghil [62] to represent the state of the tropical Pacific in a model of the El-Niño/Southern-Oscillation (ENSO) phenomenon.

(iv) An element of the system may switch from one state to another under an impact from its nearest neighbors (Fig. 1b). The dynamics of the system is controlled by the time delays between the given impact and the switching to another state.

(v) At the start, $n = 0$, all elements are in the state $(0, 0)$, intact and unloaded. Most of the changes in the state of an element occur in the following cycle:

$$(0,0) \to (0,1) \to (1,1) \to (1,0) \to (0,0) \ldots$$

However, other sequences are also possible, with one exception: a failed and loaded element may switch only to a failed and unloaded state, $(1,1) \to (1,0)$. This mimics fast stress drop after a failure.

(vi) It is supposed that all the interactions take a nonzero time. We model this by introducing four basic time delays:

- Δ_L – between an element being impacted by the load and switching to the loaded state, $(\cdot,0) \to (\cdot,1)$;
- Δ_F – between the increase in weakness and switching to the failed state, $(0,\cdot) \to (1,\cdot)$;
- Δ_D – between failure and switching to the unloaded state, $(\cdot,1) \to (\cdot,0)$;
- Δ_H – between the moment when healing conditions are established and switching to the intact (healed) state, $(1,\cdot) \to (0,\cdot)$.

In each specific case we determine a delay as described in Sect. 2.3 and 2.4 below, depending on the impact of the nearest neighbors of an element.

2.3 Load switching

The top element of the system is loaded by external forces. The load is transferred down the hierarchy, so that an element on all other levels may receive the load only from its parent and siblings. Each element may transfer the load only to its siblings and children. The load dissipates only at the lowest level. This is reminiscent of 3-D turbulence, where energy enters the system only at the largest scale, is redistributed across all scales, and is finally dissipated at the shortest scales [63].

2.3.1 Top element

(i) *Loading.* The unloaded top element becomes loaded, $(0,0) \to (0,1)$, after it remains unbroken for the time Δ_L. This delay mimics the time taken to accumulate the load from external forces.

(ii) *Unloading.* After the top element breaks down, it becomes unloaded, $(1,1) \to (1,0)$, with the time delay Δ_D. This delay mimics the time taken to release the accumulated load.

2.3.2 Other elements

Load switching for an element depends on the impact from its neighbors.

(i) *Loading.* An unloaded element becomes loaded, $(\cdot,0) \to (\cdot,1)$, under the impact from a loaded parent or siblings. This mimics the influx of load with a delay defined by (2) below.

(ii) *Unloading.* A loaded element becomes unloaded, $(\cdot,1) \to (\cdot,0)$, in two cases: First, under the impact from an unloaded parent or siblings, with the delay defined by (5) below; this mimics a deficiency of the load influx. Second, after failure with the fixed delay Δ_D; this mimics the time taken to release the accumulated load, in the same way as for the top element.

(iii) *Total impact* $I_e(n)$ on an element e at epoch n is defined as follows:

$$I_e(n) = l_p - l_e + k \sum_i (l_i - l_e). \tag{1}$$

Here the summation is taken over the indices i of the element's siblings, while the index p refers to its parent. The coefficient $k \leq 1$ determines the ratio between the impacts due to a parent and siblings.

(iv) *Time delay.* When the impact I_e becomes nonzero at epoch n, the load is switched on with the time delay

$$\Delta(n) = [\Delta_L / |I_e(n)|]\,. \tag{2}$$

Here $[x]$ denotes the integer part of x.

The impact can become zero during the delay $\Delta(n)$ given by (2); this won't affect the loading. This rule ensures that the load switching occurs sooner when the neighbors' impact is larger. When an element is loaded only by its parent we have $|I_e| = 1$ and the delay is Δ_L, the same as for the top element.

According to (1) the total impact $I_e(n)$ may change at each moment n_j, $j = 1, 2, \ldots$, when the element e, its parent, or a sibling switch their load. At each step n_j we define the corresponding epoch $N_e^{(l)}(n_j) = n_j + \Delta(n_j)$ of load switching, where $\Delta(n_j)$ is given by (2). The load actually switches at the earliest possible moment, that is for the smallest value of $N_e^{(l)}(n_j)$.

2.4 Failures

(i) *Impact of neighbors.* We assume that an element is weakened by the failure of its neighbors. The weakness W_e of element e at epoch n is defined as follows:

$$W_e(n) = cF_c(n) + (1 - c)F_s(n) + pF_p(n). \tag{3}$$

Here $F_c(n)$ and $F_s(n)$ are the numbers of failed children and siblings of the element e respectively. The Boolean function $F_p(n)$ indicates the weakening caused by the failure of a parent. The weakening takes place during the rapid transfer of the load by the parent, that is during Δ_D time units after its failure. The nonnegative coefficients c and p determine the impact of neighbor's failure.

Note that the mechanism of weakening due to the state of a parent is different from that due to siblings and children. According to (3), a child or a sibling weaken the element for as long as they are in a failed state, independently of their load; the parent does so, however, only while it is in a failed but not yet unloaded state.

(ii) *Failure.* An intact element e fails when it is loaded and its weakness exceeds a certain threshold:

$$l_e(n) = 1 \textbf{ and } W_e(n) \geq W_0(n). \tag{4}$$

After these conditions are satisfied, the element fails, i.e. the transition $(0,1) \to (1,1)$ occurs, with the time delay

$$\Delta(n) = \left\lceil \Delta_F e^{(W_0 - W_e(n))} \right\rceil. \tag{5}$$

Failure occurs if the condition (4) holds during the delay (5). The larger the difference $W_0 - W_e(n)$, the sooner the failure occurs.

(iii) *Time delay.* According to (3), the weakness $W_e(n)$ of an element e may change at each moment n_j, $j = 1, 2, \ldots$, when at least one of the element's nearest neighbors switches its state. At each step n_j we define the corresponding moment $N_e^{(s)}(n_j) = n_j + \Delta(n_j)$ of state switching, where $\Delta(n_j)$ is now given by (5). The element fails at the earliest possible moment, that is for the smallest value of $N_e^{(s)}(n_j)$, as is the case for load switching in Sect.2.3.2 above.

2.5 Healing

After its failure, and subsequent unloading, an element starts to heal. It will become intact, $(1, \cdot) \to (0, \cdot)$, after at least two of its children remain intact for the time Δ_H, independently of the element's load.

2.6 Triggering of inverse cascades

An element fails if and only if a sufficient number of its children are broken. For that reason an inverse cascade of failures can only be triggered on the lowest level of the model. For the elements on that level we imitate the number of the broken children U_e by a random process. The simplest physical reason for introducing such a process is that the hierarchical structure actually continues beneath the first level and is truncated off in our otherwise deterministic model.

Specifically, $U_e(n)$ is defined as a random walk with integer values from 0 to 3; this is the possible number of broken children in our system. The initial value for each element is $U_e(0) = 0$; increments are drawn form a Poisson process with intensity λ. An increment $+1$ or -1 appears if the element is loaded or unloaded, respectively. This ensures that the children of a loaded element are more likely to fail. The value of U_e does not change in extreme cases: when $U_e = 0$ and the increment is -1; or when $U_e = 3$ and the increment is $+1$.

Random initial states were considered in a BDE model for paleoclimate by Wright et al. [64], while the effect of periodic forcing was studied in their ENSO model by Saunders and Ghil [62]. To the best of our knowledge, the use of random forcing in a BDE model is new.

2.7 Conservation law

Our BDE model is dissipative in the usual physical sense — as well as in the mathematical sence formulated by Ghil and Mullhaupt [6] — if we associate the loading with an energy influx. The energy dissipates only at the lowest level, where it is transferred downwards, out of the model. In any part of the model that does not include its lowest level energy conservation holds, but only after averaging over sufficiently large time intervals. On small intervals it may not hold, due to the discrete time delays involved in energy transfer.

2.8 Parameters

The model has the following parameters:

- The time delays Δ_L, Δ_D, Δ_F, and Δ_H, whose dimension is time.
- The intensity λ of the random initial fracturing, with a dimension of inverse time; it controls the triggering of inverse cascades of failures (See Sect. 2.6).
- The dimensionless parameter k that determines the relative impact of the parent and siblings on the load switching; see Eq. (1). Equivalently, k detemines the load redistribution among children and siblings.
- The dimensionless parameters c and p defining how the children, siblings and parent weaken an element; with $0 \leq c \leq 1$ and $p \geq 0$; see Eq. (3).
- The weakness threshold W_0; see Eq. (4).

The time may be normalized by one of the time delays or by the inverse intensity $1/\lambda$; we normalize time by Δ_F. The coefficients c and p are normalized by the weakness threshold W_0 so that $W_0 = 1$. Accordingly, the model has seven independent parameters: $\lambda, \Delta_L, \Delta_D, \Delta_H, k, c$, and p.

In this study, the last three parameters were fixed with the values: $k = 1/3$, $c = 2/3$, and $p = 3$ (see Table 2). The ratio of the parameters Δ_H and Δ_D was kept fixed so that $\Delta_H = 2\Delta_D$. Accordingly, we concentrate on how loading Δ_L, healing Δ_H, and the forcing intensity λ affect the characteristics of our model's synthetic seismicity.

2.9 Earthquake sequence

A real-world earthquake starts with a rupture over a segment of a tectonic fault, or with nearly simultaneous rupture of several segments of the fault network. The simplest routine catalogs of observed earthquakes provide the sequence:

$$C = \{(t_k,\ m_k,\ h_k) :\ k = 1, 2, \ldots K;\ t_k \leq t_{k+1}\}\,. \tag{6}$$

Here t_k is the starting time of the rupture, m_k is the magnitude — a logarithmic measure of the energy released by the earthquake — and h_k is the position vector of the hypocenter. The latter represents a point approximation of the area where the rupture started.

In our model, an earthquake is the failure of an element or simultaneous failure of several elements. The sequence of modeled earthquakes is also represented by a "catalog" (6) with the following obvious analogies: t_k is the time of failure; m_k is the level of the broken element counted from the bottom of the hierarchy; and h_k is the position of an element within a system (see Fig. 1a). We associate h_k with the hypocenter, since this vector identifies the position of an element in relation to other elements; obviously this is a crude analogy. When a modeled earthquake comprises several broken elements, the highest of them is indicated in our catalog.

3 Multiple seismic regimes

3.1 What is a seismic regime?

A long-term pattern of seismicity within a given region is usually called a *seismic regime.* It is characterized by the frequency and the irregularity of the strong earthquakes' occurrence, namely by (i) its specific Gutenberg-Richter relation (size distribution of earthquakes); (ii) the variability of this relation with time; and (iii) the largest magnitude recorded during a few decades. The notion of seismic regime is thus a much more complete description of seismic activity than the "level of seismicity," often used to discriminate among regions with high, medium, low and negligible seismicity; the latter are called aseismic regions.

A regional seismic regime is determined by the region's neotectonics that can be described, roughly speaking, by two factors: (i) the rate of crustal deformations; and (ii) the crustal consolidation, which determines the part of the deformations that are realized through earthquakes. However, as is typical for complex processes, one long-term pattern of seismicity may switch to another in the same region, as well as migrate from one area to another on a regional or global scale [65, 66].

The term "seismic regime" is commonly used to identify the strongest, striking differences in seismicity patterns. A qualitative, heuristic definition of regimes was sufficient up till now for descriptive purposes and for the exploratory modeling done so far. Thus, the problem of formal definition did not yet arise, as good definitions often arise only after a problem is solved. The factors that determine the realization of one regime or another have been studied in [51, 67, 68, 69]. In this section we explore the distinct regimes that arise in the CC model formulated in Sect. 2.

3.2 Seismic cycles

Sequences of seismic cycles are an essential feature of observed long-term seismicity. A seismic cycle consists of three consecutive phases [33]:

1) "preseismic" rise of activity culminating in one or several major earthquakes;

2) "postseismic" gradual decline of activity; and

3) relatively low activity that eventually returns to another rise.

Such cycles take place on different time and space scales. Exact periodicity is quite rare; usually, observed time intervals between consecutive major earthquakes depart considerably from their mean, and the outlook as well as timing of a particular phase within each cycle varies strongly from cycle to cycle. At different times, seismic cycles may culminate in earthquakes of different magnitude. It is common for the sequence of cycles to exhibit intermittent behavior.

3.3 Three seismic regimes

We computed a few hundreds of earthquake sequences over the time interval $I = [0,\ 2 \cdot 10^6]$, while varying the values of parameters within the ranges given in Table 2. The sequences so obtained can be qualitatively divided into three seismic regimes. Typical examples of each regime are shown in Fig. 3. The figure's three panels are described below.

Regime **H**: *High and nearly periodic seismicity* (top panel). All cycles reach the top level, $m = L$, with $L = 6$. They are very similar and thus the sequence is approximately periodic, in the statistical sense of cyclo-stationarity [70].

Regime **I**: *Intermittent seismicity* (middle panel). The seismicity reaches the top level for some but not all cycles. The sequences are thus much less periodic than in Regime **H**.

Regime **L**: *Medium or low seismicity* (lower panel). No cycle reaches the top level and seismic activity is much more constant at a low or medium level, without the long quiescent intervals present in Regimes **H** and **I**.

Next, we explore the regimes' major characteristics and their location in parameter space.

3.3.1 Gutenberg-Richter (GR) relation

In our model, the GR relation is quite distinct from one regime to another (see Fig. 4).

For regime **H**, the relation is almost perfectly linear, $\log N(m) = a - bm$, over all possible magnitudes, with $b = 0.48$. For regimes **I** and **L** (panels b and c, respectively) the GR relation is increasingly convex and thus cannot be characterized well by a single slope b. A straight line with the slope $b = 0.48$ is shown in panels (b) and (c) for comparison.

For regime **H**, Fig. 4a, the relation is stationary, while for the other two it is changing in time (not shown).

3.3.2 The internal dynamics of the regimes

Figure 5 shows the average density $\rho(n)$ of the elements that are in a failed state at epoch n:

$$\rho(n) = \left[\nu_1(n) + \ldots + \nu_m(n)\right]/L. \tag{7}$$

Here $\nu_i(n)$ is the rate of failed elements at the i-th level of the hierarchy at the moment n, while L is the depth of the tree. The levels are counted from the bottom of the hierarchy. The panels, top to bottom, correspond to the same synthetic sequences as in Fig. 3. The density ρ exhibits the same transition from near-periodicity (panel a) to intermittent (panel b) and eventually to low-level noisy behavior (panel c) as in Fig. 3.

3.3.3 Regime diagram

The location of the regimes in the plane of the two key parameters (Δ_L, Δ_H) is shown in Fig. 6. The values of Δ_L and Δ_H vary as shown in the figure, while the rest of the parameters have the fixed values given in the caption to Fig. 3.

The high-seismicity, nearly periodic regime **H** occurs predominantly for high values of Δ_H, that is for low healing rates. The low-seismicity, noisy regime **L** occurs for low Δ_H and high Δ_L — i.e., for high healing rates and very slow loading. The intermittent regime **I** occurs for low Δ_H and low Δ_L, when both the healing and loading rates are high. The domain of the regime **I** extends also toward the upper right edge of the figure and fades away as it approaches the *triple point* at which all three regimes meet.

The three sequences shown in Fig. 3 correspond to the three stars in Fig. 6 at fixed

$\Delta_L = 0.5 \cdot 10^4$ and increasing Δ_H.

Next, we analyze what happens to the system when it is driven across regime boundaries.

3.3.4 Measure of seismicity clustering

To better describe the differences between regimes, we define a measure G of clustering. This is done in the following steps.

(i) First, we define a measure $\Sigma(I)$ of seismic activity within the time interval I as

$$\Sigma(I) = \frac{1}{n}\sum_{i=1}^{n} 10^{am_i}, \ a = \log_{10} 3. \tag{8}$$

Here summation is taken over all events that occur within the time interval I, i is the sequential index of an event, and m_i is the magnitude of the i-th event. The value of a equalizes, on average, the contribution of earthquakes with different magnitudes, that is from different levels of the hierarchy.

(ii) Consider a subdivision of a time interval I into a set of nonoverlapping intervals of length $\epsilon > 0$. For simplicity we choose ϵ such that $|I| = \epsilon N_I$, where $|\cdot|$ denotes the length of an interval and N_I is an integer. Therefore, we have the following representation:

$$I = \bigcup_{i=1}^{N_I} I_i, \ |I_j| = \epsilon, j = 1, \ldots, N_I, \ I_i \cap I_j = \emptyset, i \neq j. \tag{9}$$

(iii) For each $n = 1, \ldots, N_I$ we choose an n-subset $\Omega(n) = \left\{\bigcup_{i=m_1,\ldots,m_n} I_i\right\}$ of the total covering set (9) that maximizes the value of Σ obtained over the possible subsets of total length n, i. e.,:

$$\max_{j=i_1,\ldots,i_n} \{\Sigma(\cup I_j)\} = \Sigma(\Omega(n)) \equiv \Sigma^*(n). \tag{10}$$

(iv) Introducing the notations

$$\bar{\Sigma}(n) = \Sigma^*(n)/\Sigma(I), \;\; \tau(n) = n\epsilon/|I|, \tag{11}$$

we finally define the measure of clustering within the interval I as

$$G(I) = \max_{n=1,\dots,N_I} (\bar{\Sigma}(n) - \tau(n)). \tag{12}$$

Figure 7 illustrates the behavior of the clustering measure $G(I)$ so defined. Panel (a) shows $\bar{\Sigma}$ vs. τ for the three synthetic sequences shown in Fig. 3. The more clustered the sequence, the more convex the corresponding curve. A marked Poisson process with independent marks would correspond, for appropriate ϵ, to a diagonal line that depicts the absence of clustering.

Figure 7b displays the curves $\bar{\Sigma} - \tau$ vs. τ and the corresponding maxima of G for the three synthetic sequences shown in Fig. 3.

The measure G is used next to depict a bifurcation in our system's behavior during the transition from Regime **H** to Regime **L**.

3.3.5 Transitions between regimes in parameter space

Figure 8 illustrates the transition between regimes in the parameter plane (Δ_L, Δ_H). Panel (a) shows a rectangular trajectory in this plane that passes through all the three regimes and touches their triple point. We single out the 30 points along this trajectory, that are indicated by small circles in the figure. The three pairs of points that correspond to the transitions between regimes are distinguished by large circles and marked in addition by letters, for example (A) and (B) mark the transition from Regime **H** to Regime **L**.

We estimate the clustering $G(I)$, $I = [0, 2 \cdot 10^6]$ for the synthetic sequences that correspond to the 30 marked points along the trajectory in Fig. 8a. Figure 8b shows the corresponding values of G. We see the dramatic drop, from 0.8 to 0.18, between points (A) and (B) that correspond to the transition from Regime **H** to Regime **L**. The values of G remain small, $G \approx 0.1$, in Regime **L**, between points (B) and (C).

The transition (C)–(D) that leads to Regime **I** is very smooth, unlike that from **H** to **L**. The clustering G increases from 0.1 to 0.53 while the trajectory is moving across Regime **I**, from point (D) to (E). The transition (E)–(F) is again smooth and G increases further, albeit more gradually. Finally, it reaches the level $G = 0.8$ and fluctuates around it while the trajectory advances through the domain of Regime **H**, between points (F) and (A).

The transition between regimes is illustrated in greater detail in Fig. 9. It shows fragments of the six synthetic sequences that correspond to the points (A)–(E) in Fig. 8a. The sharp difference in the character of seismicity between points (A) and (B), near the boundary between Regimes **H** and **L**, is even more obvious than in Fig. 8b. The other two transitions, from (C) to (D) and (E) to (F), are much smoother, but they still highlight the intermittent character of Regime **I**.

Figures 8 and 9 quantify and illustrate the bifurcation in system's dynamics that occurs in parameter space on the boundary between Regimes **H** and **L**. The abrupt change in earthquake clustering there is well expressed by the measure G of Eq. (12). The more subtle change in intermittency that occurs at the boundaries **L**–**I** and **I**–**H** awaits better quantification in subsequent work.

3.3.6 Intermittent regime

We explore here in a greater detail the intriguing intermittent regime **I**. Figure 10 shows different patterns of intermittency obtained by varying the parameters Δ_L and Δ_H. The sequences shown in panels (a)–(f) of Fig. 10 correspond to points (a)–(f) in the plane (Δ_L, Δ_H) of Fig. 6. The rest of the parameters are fixed at the values given in the caption. Two sequences, (a) and (b), are taken from Regime **H**, for comparison purposes; the other four, (c)-(f), are from Regime **I**.

The sequence in panel (a) consists of nearly periodic cycles, all of which end with an event of magnitude $m = 6$; there is no intermittency. In panel (b) the activity between cycles starts to rise. This sequence lies in the near near vicinity of the boundary between regimes **H** and **I** (see Fig. 6).

Panel (c) shows the developed intermittency. One can see within this sequence three types of behavior: (i) nearly periodic cycles that end with events of magnitude $m = 6$ and exhibit no intercycle activity (see for instance the time interval $5.6 \cdot 10^5 \leq t \leq 5.8 \cdot 10^5$), like in panel (a); (ii) nearly periodic cycles that end with events of lower magnitudes and are separated by varying intercycle intervals (e. g. $4.3 \cdot 10^5 \leq t \leq 4.8 \cdot 10^5$); and (iii) cycles that always end with events of magnitude $m = 6$ but display very strong intercycle activity of variable duration (e.g. $3.5 \cdot 10^5 \leq t \leq 4.0 \cdot 10^5$). The timing and duration of these three types of behavior appear to vary randomly with time.

Panel (d) illustrates a case when cycles culminating by strong earthquake with $m = 6$ occur only very rarely. Most of the cycles end with lower magnitudes. This is due to the fact that we approach the domain of Regime **M** (see Fig. 6). Panel (e) represents a sequence with very long intervals of nearly periodic cycles that differ in mean period and end with different magnitudes. Note that the three sequences shown in panels (c), (d) and (e) are close neighbors in parameter space (see Fig. 6). Nevertheless, they demonstrate a rich variety of long-term seismicity outlooks. This is always the case near the triple point, where the system is very sensitive to small changes in parameter values.

Panel (f) shows one of the most interesting situations. All cycles are periodic and end with events of magnitude $m = 6$. But the length of the cycles themselves, as well as that of intercycle intervals, are quite irregular.

Figure 11 gives the mean density $\rho(n)$ of failures at a given epoch for the sequences shown in Fig. 10. The simple, near-cyclical behavior in panels (a) and (b) changes to a much more irregular behavior in panels (c) and (d), while the one in panels (e) and (f) is quite intermittent. The latter alternates in an entirely unpredictable and whimsical manner between different amplitudes and periods over time.

4 Physics of regime switching

We now discuss qualitatively the mechanisms that may determine the realization of one or another seismic regime in the present model.

4.1 Memory

The formation of different regimes in the model has a simple physical explanation in terms of the system's memory. It may be qualitatively characterized as follows. Consider two snapshots of the system, showing the state of each element at the moments n and $n + s$; the four possible states of an element are given in Table 1. Memory is "short" if the correlation between the snapshots is rapidly decreasing with s and "long" if the decrease is slow.

When the system has a long memory its current state strongly affects its subsequent evolution. In this case, behavior that falls in the intermittent regime **I** is formed.

Short memory can lead to a sequence of ceismic cycles that belongs to one of the regimes **H** or **L**, depending on loading and healing rates. When the regime **H** is realized it consists of statistically equivalent, independent seismic cycles that end with the largest possible magnitude. Regime **L** comprises a mixture of independent low-level cycles; it thus exhibits noisy behavior.

4.2 Role of parameters

The model's effective memory, and therefore the resulting regime, is determined by the interplay of parameters. Generally speaking, the changes in the system become faster, and memory shorter, when the initial-fracturing parameter λ (see Sec. 2.6) increases — so the inverse cascades become more intensive — and when either of the four time delays decreases. This situation will favor, therefore, the appearance of regimes **H** or **I**.

The maximal magnitude of the earthquakes decreases with $\Delta_D + \Delta_H$, which equals the minimal time delay for healing. This will lead to preponderece of sequences that fall in the **I** or **M** regime.

4.3 Healing and loading

Healing and loading clearly play an important role in the formation of seismic regimes. Without healing ($\Delta_H = \infty$) the whole system fails in finite time and does not recover at all, as it happens in the case of the fiber-bundle model [71, 72]. When healing is slow, $\Delta_H \gg 1$, the system can recover between consecutive total failures thus creating seismic cycles, albeit very long ones. Finally, with fast healing, low-level failures heal so quickly that they can't merge to generate the larger ones. As a result, the inverse cascade never reaches the top level.

In our model, a permanent load influx drives the whole system and is the only reason for failures to start. Seismic activity thus increases with the loading rate, which is inversly proportional to Δ_L.

The role of each single parameter in the formation of a regime is therewith transparent. Note however, that the realization of a seismic sequence that falls in one regime or another depends on the interplay of parameters: no single parameter alone controls the behavior of the system.

5 Discussion

Applying the framework of Boolean delay equations (BDEs) to the modeling of colliding cascades did reach its goal: the system's dynamics becomes physically more transparent and easier to study exhaustively. BDEs may thus serve as a "missing link" for understanding how the elementary interactions within the system determine its global behavior.

Our BDE model of colliding cascades reproduces the broad spectrum of observed seismic regimes, including intermittency. Similar regimes are encountered in many other systems, for example, in economics.

The results raise the possibility of modeling intermittency in time as well as in parameter space. This may provide a base for the study of the next problem: prediction of regime switching. The memory of the system may be a useful control parameter in that problem.

Regime switching is well known and intensively studied in climatology [73, 74, 75, 76, 77], as well as in many other fields. Similar phenomena arise in percolation theory [78], as well as in its application to forest fire models [79]: the existence of an infinite percolation cluster is analogous to rupture of the top element in the system considered here. In that way, regime switching could be akin to phase transitions studied in statistical physics. A meaningful connection, if any, is yet to be established, however.

Our three regimes **H**, **I** and **L** are naturally associated with *catastrophic*, *self organized critical* and *stable* regimes that have been found analytically by Shnirman and Blanter [61, 69] for a static hierarchical model of defect development with only an inverse cascade of fracturing. They have found an asymptotic distribution of regimes as a function of the inhomogeneity in model strength. The existence of these analytically obtained regimes is thus well confirmed by our dynamical simulations.

The second part of this paper extends our study to the earthquake prediction problem. We demonstrate in it that the model considered, its simplicity notwithstanding, does reproduce a broad variety of the premonitory seismicity patterns observed in reality.

Acknowledgments

It is a pleasure to acknowledge numerous discussions with many colleagues. The work of I.Z. and V.K.-B. was supported by The 21st Century Collaborative Activity Award for Studying Complex Systems from James S. McDonnel foundation. M.G.'s work was supported by NSF grant ATM-0082131.

References

[1] Gabrielov, A., Keilis-Borok, V., Zaliapin, I., and Newman, W.I., 2000. Critical transitions in colliding cascades, Phys. Rev. E, 62, 237-249.

[2] Gabrielov, A.M., Keilis-Borok, V.I., Zaliapin, I.V., and Newman, W.I., 2000. Colliding cascades model for earthquake prediction. J. Geophys. Intl., 143, 427-437.

[3] Gabrielov, A. Zaliapin, I., and Keilis-Borok, V., 2001. Premonitory seismicity patterns in cellular automata with colliding cascades. Manuscript.

[4] Shebalin, P., Zaliapin, I., and Keilis-Borok, V., 2000. Premonitory raise of the earthquakes' correlation range: Lesser Antilles. Phys. Earth Planet. Int., 122, 241-249.

[5] Dee, D., and Ghil, M., 1984. Boolean difference equations, I: Formulation and dynamic behavior. SIAM J. Appl. Math. 44, 111-126.

[6] Ghil, M. and Mullhaupt, A. P., 1985. Boolean delay equations. II: Periodic and aperiodic solutions. J. Stat. Phys. 41, 125-173.

[7] Zaliapin, I., Keilis-Borok, V., and Ghil, M., 2001. A Boolean Delay Equation Model of Colliding Cascades. Part II: Prediction of Critical Transitions. Manuscript.

[8] Ghil, M., Mullhaupt A., and Pestiaux, P., 1987. Deep water formation and Quaternary glaciations, Climate Dyn., 2, 1-10.

[9] Ghil, M., and Childress, S. 1987. Topics in Geophysical Fluid Dynamics: Atmospheric Dynamics, Dynamo Theory and Climate Dynamics, Springer-Verlag, New York/Berlin/London/Paris/ Tokyo.

[10] Keilis-Borok, V. I., 1990. The lithosphere of the Earth as a non-linear system with implications for earthquake prediction. Rev. Geophys., 28, 19-34.

[11] Smale, S., 1967. Differentiable dynamical systems. Bull. Amer. Math. Soc. 73, 747-817.

[12] Arnol'd, V. I., 1983. Geometrical Methods in the Theory of Ordinary Differential Equations. Springer-Verlag, New York.

[13] Hénon, M., 1966. La topologie des lignes de courant dans un cas particulier. C. R. Acad. Sci. Paris. 262, 312-414.

[14] Collet, P., and Eckmann, J.-P., 1980. Iterated Maps on the Interval as Dynamical Systems. Birkh´auser Verlag, Basel/Boston.

[15] Wolfram, S., 1994. Cellular Automata and Complexity: Collected Papers. Addison-Wesley, Reading, Mass.

[16] Gutowitz, H., 1991. Cellular Automata: Theory and Experiment. MIT Press, Cambridge, MA.

[17] Emiliani C. and Geiss, J., 1957. On glaciations and their causes. Geol. Rundschau. 46, 576-601.

[18] Broecker, W. S., Peteet, D. M. and Rind, D., 1985. Does the ocean-atmosphere system have more than one stable mode of operation? Nature. 315, 21-25.

[19] Imbrie, J., Berger, A., Boyle, E. A., Clemens, S. C., Duffy, A., Howard, W. R., Kukla, G., Kutzbach, J., Martinson, D. G., McIntyre, A., Mix, A. C., Molfino, B., Morley, J. J., Peterson, L. C., Pisias, N. G., Prell, W. L., Raymo, M. E., Shackleton, N. J., and Toggweiler, J. R., 1993. On the structure and origin of major glaciation cycles 2: The 100,000-year cycle. Paleoceanography 8, 699-735.

[20] Mysak, L. A., Manak, D. K., and Marsden, R. F., 1990. Sea-ice anomalies observed in the Greenland and Labrador Seas during 1901-1984 and their relation to an interdecadal Arctic climate cycle. Climate Dyn., 5, 111-113.

[21] Ghil, M., 1994. Cryothermodynamics: The chaotic dynamics of paleoclimate, Physica D, 77, 130-159.

[22] Ghil, M., and Robertson, A. W., 2000. Solving problems with GCMs: General circulation models and their role in the climate modeling hierarchy. General Circulation Model Development: Past, Present and Future , D. Randall (Ed.), Academic Press, San Diego, pp. 285-325.

[23] Jacob, F. and Monod, J., 1961. Genetic regulatory mechanisms in the synthesis of proteins. J Molecular Biol. 3, 318-356.

[24] Thomas, R., 1979. Kinetic Logic: A Boolean Approach to the Analysis of Complex Regulatory Systems. Springer-Verlag, Berlin/New York.

[25] Nicolis, C., 1982. Boolean approach to climate dynamics. Q. J. R. Meteorol. Soc. 108, 707-715.

[26] Kauffman, S. A., 1969. Metabolic stability and epigenesis in randomly constructed genetic nets. J. Theor. Biol. 22, 437-467.

[27] Cowan, G. A., Pines, D. and Melzer, D. (Eds.), 1994. Complexity: Metaphors, Models and Reality. Addison-Wesley, Reading, Mass.

[28] Kauffman, S. A., 1995. At Home in the Universe: The Search for Laws of Self-Organization and Complexity. Oxford University Press, New York.

[29] Darby M. S., and Mysak, L. A., 1993. A Boolean delay equation model of an interdecadal Arctic climate cycle. Climate Dyn., 8, 241-246.

[30] Gelfand, I. M., Guberman, Sh. A., Keilis-Borok, V. I., Knopoff, L., Press, F., Ranzman, E. Ya., Rotwain, I. M., and Sadovsky, A. M., 1976. Pattern recognition applied to earthquake epicenters in California. Phys. Earth Planet. Int., 11, 227-283.

[31] Alekseevskaya, M., Gabrielov, A., Gelfand, I., Gvishiani, A., and Rantsman, E., 1977. Formal morphostructural zoning of mountain territories. J. Geophys. Res., 43, 227-233.

[32] Keilis-Borok, V. I., 1996. Intermediate-term earthquake prediction. Proc. Natl. Acad. Sci. USA, 93, 3748-3755.

[33] Scholz, C. H., 1990. The Mechanics of Earthquakes and Faulting. Cambridge University Press, Cambridge.

[34] Turcotte, D. L., 1997. Fractals and Chaos in Geology and Geophysics, 2nd ed. Cambridge University Press, Cambridge.

[35] Varnes, D. J., 1989. Predicting earthquakes by analysing acceleration of precursory seismic activity. Pure Appl. Geophys., 130, 661-686.

[36] Keilis-Borok, V. I. (Ed.) 1990. Intermediate-term earthquake prediction: models, phenomenology, worldwide tests. Phys. Earth Planet. Int., 61, 144.

[37] Keilis-Borok, V. I. and Shebalin, P. N. (Eds.), 1999. Dynamics of Lithosphere and Earthquake Prediction. Phys. Earth Planet. Int. 111, 179-330.

[38] Bufe, C. G. and Varnes, D. J., 1993. Predictive modeling of the seismic cycle of the greater San Francisco bay region. J. Geophys. Res., 98, 9871-9883.

[39] Burridge, R. and Knopoff, L., 1967. Model and theoretical seismicity, Bull. seism. Soc. Am., 57, 341-371.

[40] Allegre, C. J., Le Mouel, J. L., and Provost, A., 1982. Scaling rules in rock fracture and possible implications for earthquake prediction. Nature, 297, 47-49.

[41] Bak, P., Tang, C. and Wiesenfeld, K., 1988. Self-organized criticality. Phys. Rev. A 38, 364-374.

[42] Narkunskaya, G. S. and Shnirman, M. G., 1990. Hierarchical model of defect development and seismicity. Phys. Earth. Planet. Inter., 61, 29-35.

[43] Newman, W. I., Gabrielov, A., and Turcotte, D. L. (Eds.), 1994. Nonlinear Dynamics and Predictability of Geophysical Phenomena, Geophys. Monographs Ser. 83. AGU, Washington, DC.

[44] Rundle, J. B., Turcotte, D. L. and Klein, W. (Eds.), 2000. Geocomplexity and the Physics of Earthquakes. American Geophysical Union, Washington, DC.

[45] Turcotte, D. L., Newman, W. I., and Gabrielov, A., 2000. A statistical physics approach to earthquakes. In: J. B. Rundle, D. L. Turcotte, and W. Klein. (Eds.), Geocomplexity and the Physics of Earthquakes. Am. Geophys. Un., Washington, DC, pp. 83-96.

[46] Barenblatt, G. I., 1993. Micromechanics of fracture. In: Theoretical and Applied Mechanics, Bodner, E. R., Singer, J., Solan, A., and Hashin, Z. (Eds.) Elsevier, Amsterdam, pp. 25-52.

[47] Holland, J. H., 1995. Hidden Order: How Adaptation Builds Complexity. Reading, MA: Addison-Wesley.

[48] Huang, Y., Saleur, H., Sammis, C., and Sornette, D., 1998. Precursors, aftershocks, criticality and self-organized criticality. Europhys. Lett. 41, 43-48.

[49] Shaw, B.E., Carlson, J.M., and Langer, J.S., 1992. Patterns of seismic activity preceding large earhquakes. J. Geophys. Res. 97, 479.

[50] Allegre, C. J., Le Mouel, J. L., Ha Duyen, C., and Narteau, C., 1995. Scaling Organization of Fracture Tectonics (S. O. F. T.) and Earthquakes Mechanism. Phys. Earth Planet. Int., 92, 215-233.

[51] Dahmen, K., Ertas, D. and Ben-Zion, Y., 1998. Gutenberg-Richter and characteristic earthquake behavior in simple mean-field models of heterogeneous faults. Phys. Rev. E, 58, 1494-1501.

[52] Gabrielov, A., Newman, W. I., and Turcotte, D. L., 1999. An exactly soluble hierarchical clustering model: inverse cascades, self-similarity and scaling. Phys. Rev. E, 60, 5293-5300.

[53] Gabrielov, A. and Newman, W. I. Seismicity modeling and earthquake prediction: A review. 1994. In W. I. Newman, A. Gabrielov, and D. L.Turcotte (Eds.), Nonlinear Dynamics and Predictability of Geophysical Phenomena. Am. Geophys. Un., Int. Un. of Geodesy and Geophys., 7-13 (Geophysical Monograph 83, IUGG Vol. 18).

[54] Gabrielov, A., Newman, W. I., and Knopoff, L., 1994. Lattice models of failure: Sensitivity to the local dynamics. Phys. Rev. E., 50, 1, 188-197.

[55] Turcotte, D. L., Malamud, B. D., Morein, G., and Newman, W. I., 1999. An inverse cascade model for self-organized criticality. Physica A, 268, 629-643.

[56] Rundle, J. B., Klein, W. and Tiampo, K., 2000. Linear pattern dynamics in nonlinear threshold systems. Phys. Rev. E, 61, 2418-2431.

[57] Rundle, J. B., Gross, S., Klein, W., Ferguson C. D., and Turcotte, D. L., 1997. The statistical mechanics of earthquakes. Tectonophysics, 277, 147-164.

[58] Sammis, C. G., Sornett, D., and Saleur, H., 1996. Complexity and earthquake forecasting. In: Rundle, J. B., Turcotte, D. L., and Klein, W. (Eds.) SFI Studies in the Science of Complexity, v. XXV, Addison-Welsey.

[59] Sornette, D., 1999. Complexity, catastrophe and physics. Physics World 12, 57.

[60] Sornette, D., 1998. Multiplicative processes and power laws. Phys. Rev. E 57, 4811-4813.

[61] Blanter, E. M. and Shnirman, M. G., 1997. Simple hierarchical systems: stability, self-organised criticality and catastrophic behaviour. Phys. Rev. E, 55(6), 6397-6403.

[62] Saunders A. and Ghil, M., 2001. A Boolean delay equations model of ENSO variability. Physica D, sub judice.

[63] Frisch, U., 1995. Turbulence: The Legacy of A. N. Kolmogorov. Cambridge University Press, 343 pp.

[64] Wright, D. G., Stocker, T. F., and Mysak, L. A., 1990, A note on Quaternary climate modelling using Boolean delay equations. Climate Dyn., 4, 263-267.

[65] Press, A., and Allen, C., 1995. Pattern of seismic release in the southern California region. J. Geophys. Res., 100, 6421-6430.

[66] Romanowicz, B., 1993. Spatiotemporal patterns in the energy-release of great earthquakes. Science, 260, 1923-1926.

[67] Ben-Zion, Y., Dahmen, K., Lyakhovsky, V., Ertas, D., and Agnon, A., 1999. Self-driven mode switching of earthquake activity on a fault system. Earth Planet. Sci. Lett., 172, 11-21.

[68] Newman, W. I. and Knopoff, L., 1983. A model for repetitive cycles of large earthquakes, Geophys. Res. Lett., 10, 305-308.

[69] Shnirman, M. G. and Blanter, E. M., 1999. Mixed hierarchical model of seismicity: scaling and prediction. Phys. Earth Planet. Int., 111, 295-304.

[70] Mertins, A., 1999. Signal Analysis: Wavelets, Filter Banks, Time-Frequency Transforms and Applications. John Wiley and Sons, Chichester.

[71] Newman, W. I., Turcotte, D. L., and Gabrielov, A., 1995. Log-periodic behavior of a hierarchical failure model with applications to precursory seismic activation. Phys. Rev. E, 52, 4827-4835.

[72] Newman, W. I. and Gabrielov, A., 1991. Failure of hierarchical distributions of fiber bundles. I. Intl. J. Fracture, 50, 1-14.

[73] Smyth, P., Ide, K., and Ghil, M., 1999. Multiple regimes in Northern Hemisphere height fields via mixture model clustering. J. Atmos. Sci., 56, 3704-3723.

[74] Robertson, A. and Ghil, M., 1999. Large-scale weather regimes and local climate over the estern United States. J. Climate, 12, 1796-1813.

[75] Weeks, E. R., Tian, Y., Urbach, J. S., Ide, K., Swinney, H., and Ghil, M., 1997. Transitions between blocked and zonal flows in a rotating annulus with topography. Science, 278, 1598-1601.

[76] Kimoto, M. and Ghil, M., 1993. Multiple flow regimes in the Northern Hemisphere winter. Part I: Methodology and hemispheric regimes. J. Atmos. Sci., 50, 2625-2643.

[77] Kimoto, M. and Ghil, M., 1993. Multiple flow regimes in the Northern Hemisphere winter. Part II: Sectorial regimes and preferred transitions. J. Atmos. Sci., 50, 2645-2673.

[78] Stauffer, D. and Aharony, A., 1992. Introduction to Percolation Theory, 2nd ed., Taylor and Francis, London, 181pp.

[79] Malamud, B. D., Morein, G., and Turcotte, D. L., 1998. Forest fires: an example of self-organized critical behavior. Science, 281, 1840-1842.

Table 1. Truth table for the state of an element.

s_e	l_e	*Element's state*
0	0	*intact and unloaded*
0	1	*intact and loaded*
1	0	*failed and unloaded*
1	1	*failed and loaded*

Table 2. Fixed values of the model's parameters or their range of variation.

	λ	Δ_L	Δ_H	Δ_D	Δ_F	k	c	p	L
From	10^{-7}	1	1	0.5					
					10^3	1/3	2/3	3	6
To	10^{-2}	10^6	10^6	$0.5 \cdot 10^6$					

List of Figures

to the synthetic sequences shown in Fig. 3. Top panel – Regime **H**; middle panel – Regime **I**; and bottom panel – regime **L**.

Figure 6. Regime diagram in the (Δ_L, Δ_H) plane of the loading and healing delays. Stars correspond to the sequences shown in Fig. 3. The points (a)–(f) correspond to the sequences shown in Figs. 10 and 11.

Figure 7. Measure $G(I)$ of seismicity clustering; see Eq. (12). The three curves correspond to the three synthetic sequences shown in Fig. 3. a) Seismic activity, $\bar{\Sigma}$ vs. the fraction τ of the total time; see Eq. (11); b) the difference $\bar{\Sigma} - \tau$ vs. τ and the maximum values of G that are obtained.

Figure 8. Bifurcation diagram. a) Closed trajectory in the parameter plane of Fig. 6; b) the measure G of clustering illustrated in Fig. 7, calculated along the trajectory shown in panel (a). Bifurcation happens between points (A) and (B) for transition between regimes **H** and **L**. See details in the text; note that the points (A)–(F) here are disctinct from points (a)–(f) in Fig. 6.

Figure 9. Synthetic sequences corresponding to the points along the trajectory in parameter space (Fig. 8a.) The panels illustrate the transitions between the regimes **H** and **L** — panels (A) and (B); **L** and **I** — (C) and (D); and **I** and **H** — (E) and (F). A bifurcation occurs in the transition from (A) to (B), while the other two transitions are smoother.

Figure 10. Different types of intermittent behavior. Each panel shows a fragment of a synthetic sequence generated by our model; the time interval $[3.5 \cdot 10^5 \;\; 6.5 \cdot 10^5]$ is

shown. Differerent panels correspond to different values of the parameters Δ_L and Δ_H, as indicated in Fig. 6; the rest of the parameters are fixed: $c = 2/3, p = 3, k = 1/3, T_H = 1, \lambda = 0.2 \cdot 10^{-4}, \Delta_F = 10^3$, (a) $\Delta_L = 10^2$, $\Delta_H = 10^3$; (b) $\Delta_L = 10^3$, $\Delta_H = 7 \cdot 10^2$; (c) $\Delta_L = 5 \cdot 10^2$, $\Delta_H = 2 \cdot 10^2$; (d) $\Delta_L = 10^3$, $\Delta_H = 2 \cdot 10^2$; (e) $\Delta_L = 5 \cdot 10^2$, $\Delta_H = 10^2$; and (f) $\Delta_L = 10$, $\Delta_H = 10^2$.

Figure 11. Intermittence of seismic regimes: density of failures. Each panel shows the density of fractured elements $\rho(n)$. for the different synthetic sequences; compare Fig. 5. The parameter values for each panel and the notations are the same as in Fig. 10.

(a)

(b)

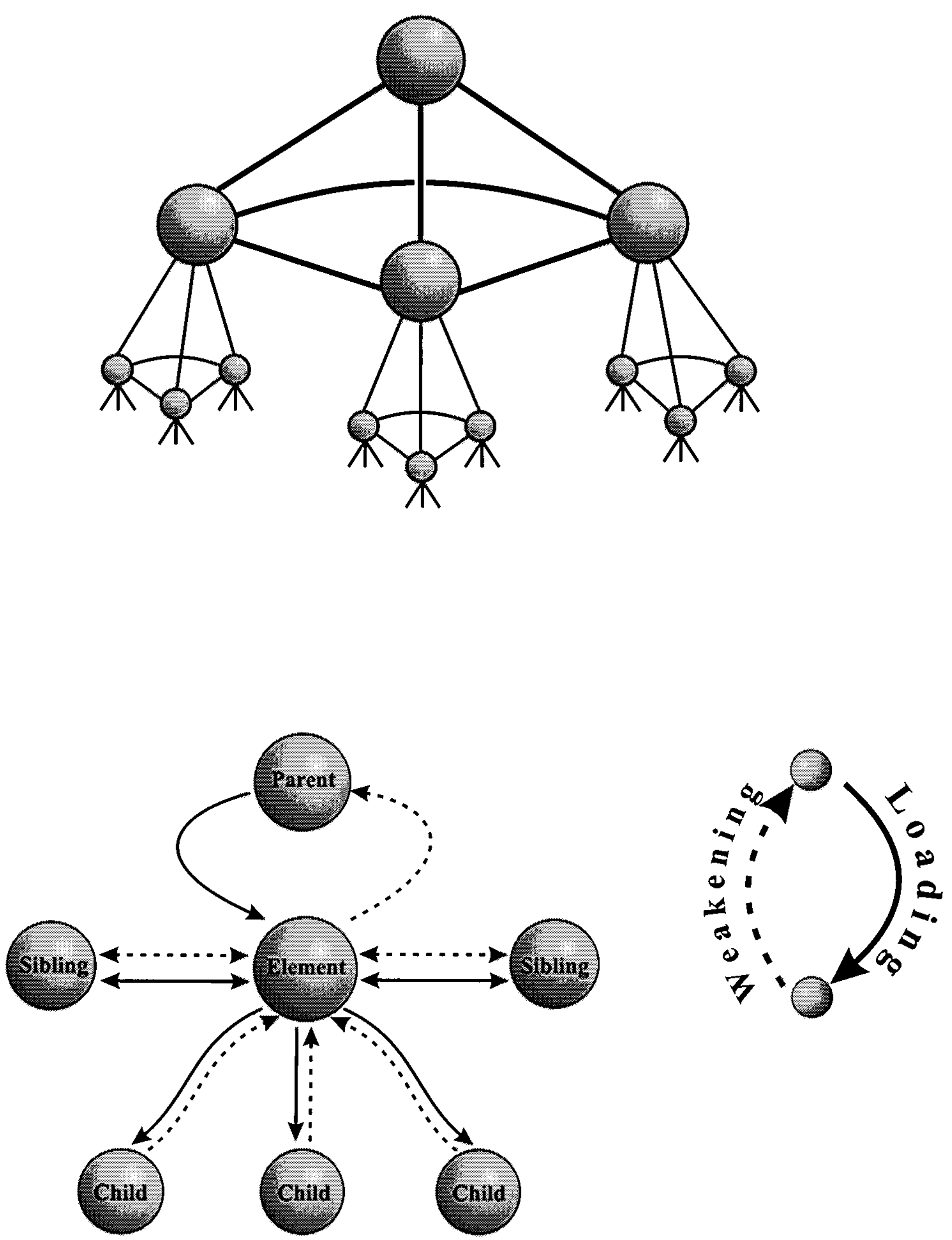

Fig. 1

CCM-BDE 2001. Part I.
I. Zaliapin, V. Keilis-Borok, M. Ghil

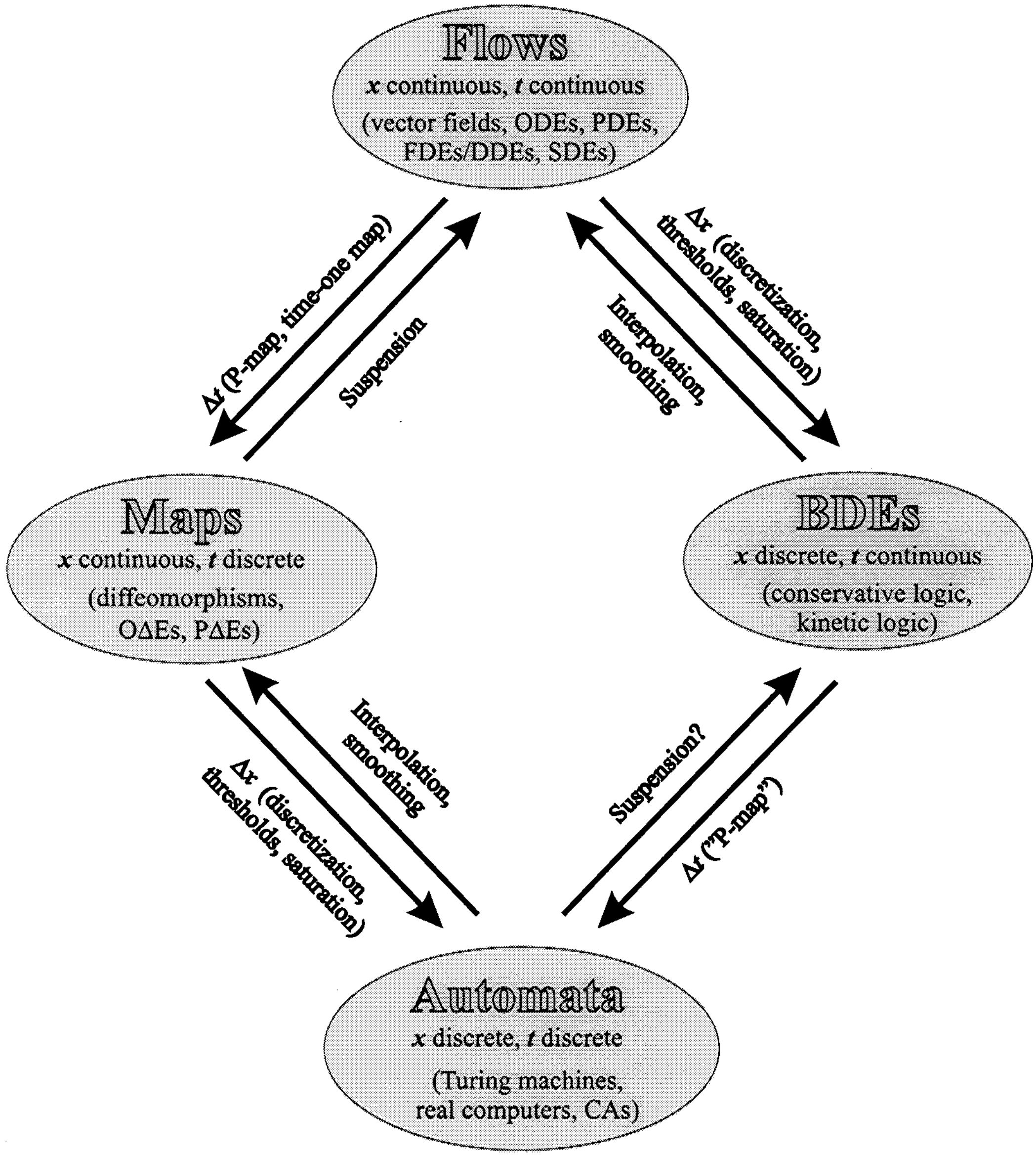
Flows
x continuous, t continuous
(vector fields, ODEs, PDEs, FDEs/DDEs, SDEs)
Δt (P-map, time-one map)
Suspension
Δx (discretization, thresholds, saturation)
Interpolation, smoothing
Maps
x continuous, t discrete
(diffeomorphisms, OΔEs, PΔEs)
BDEs
x discrete, t continuous
(conservative logic, kinetic logic)
Interpolation, smoothing
Δx (discretization, thresholds, saturation)
Suspension?
Δt ("P-map")
Automata
x discrete, t discrete
(Turing machines, real computers, CAs)

Fig. 2

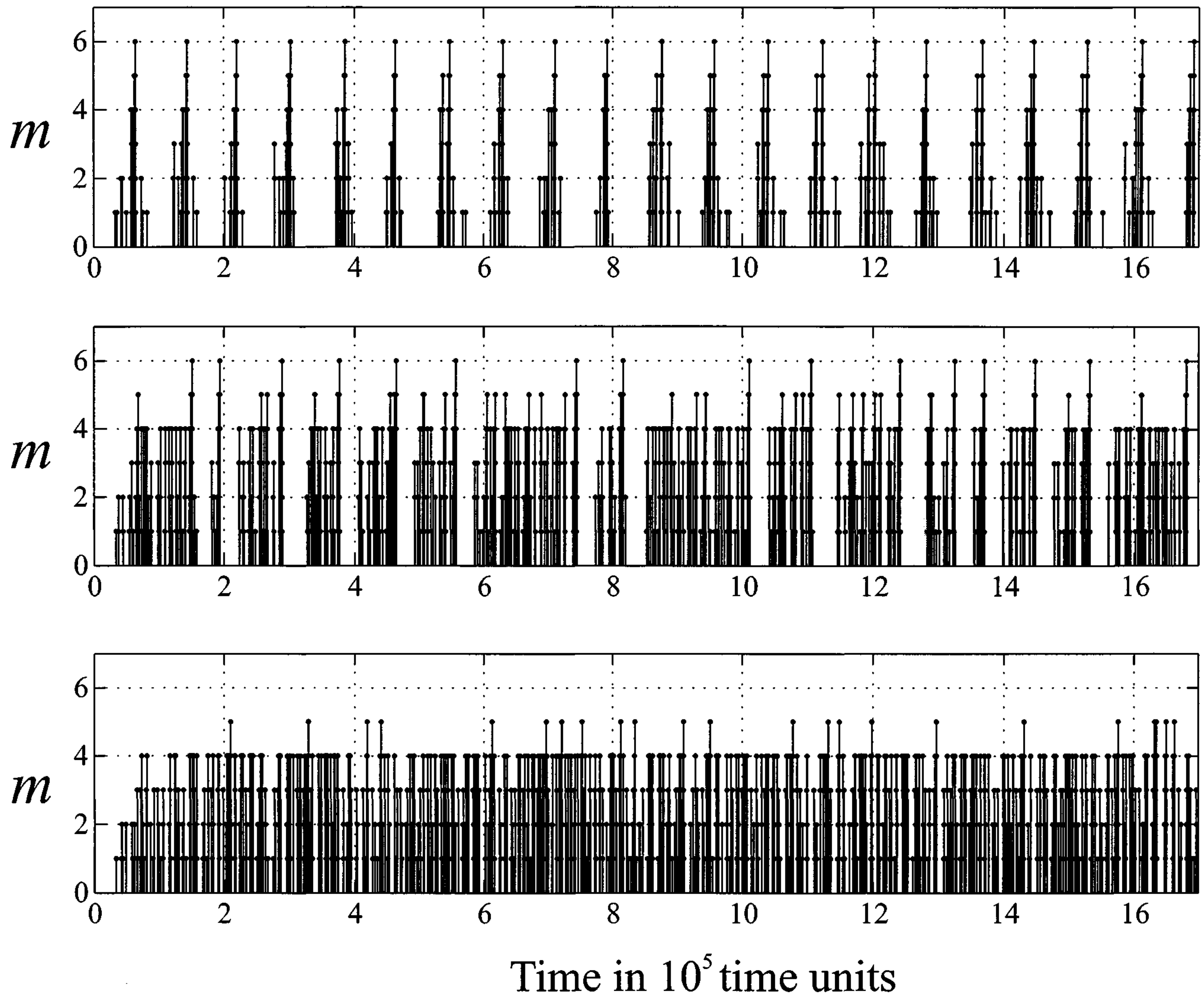

Fig. 3

CCM-BDE 2001. Part I.
I. Zaliapin, V. Keilis-Borok, M. Ghil

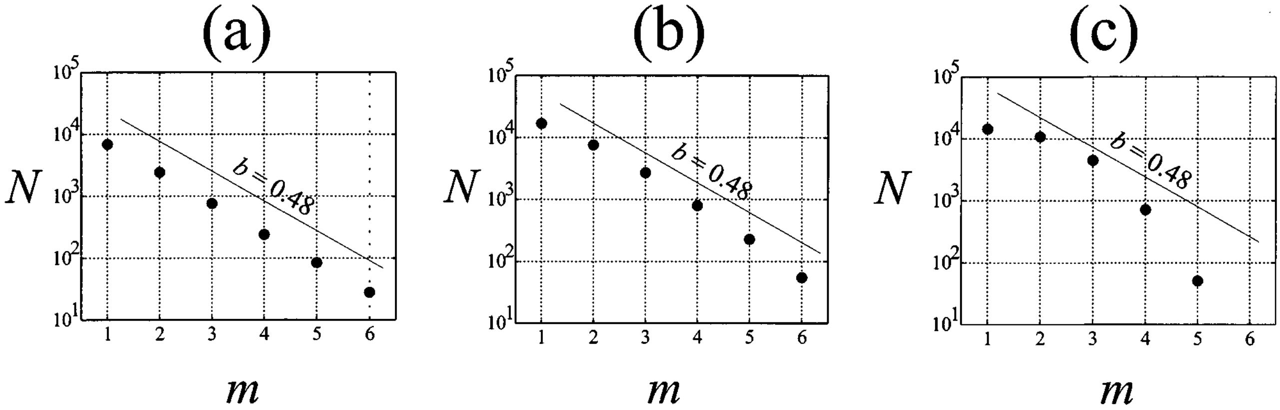

Fig. 4

CCM-BDE 2001. Part I.
I. Zaliapin, V. Keilis-Borok, M. Ghil

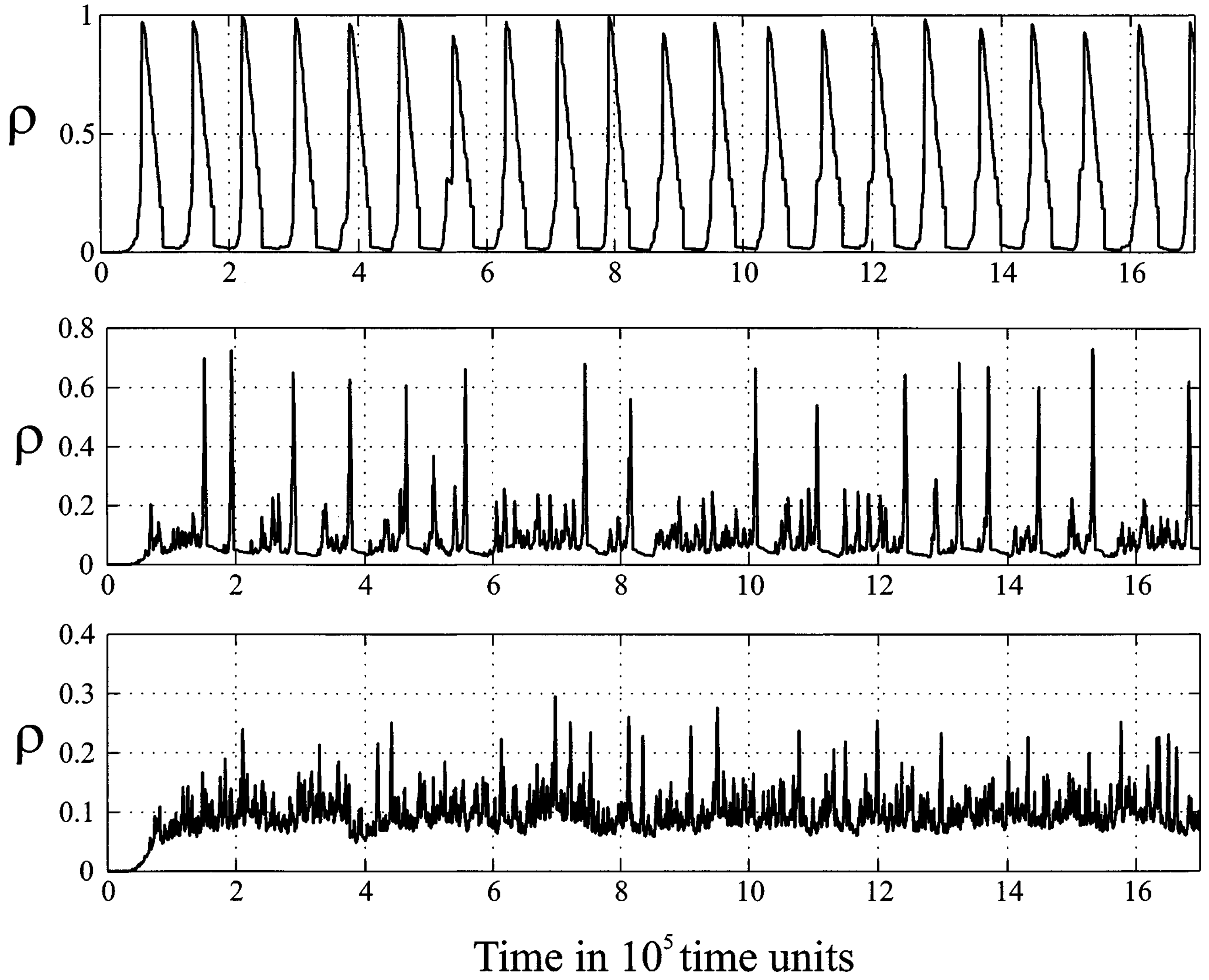

Fig. 5

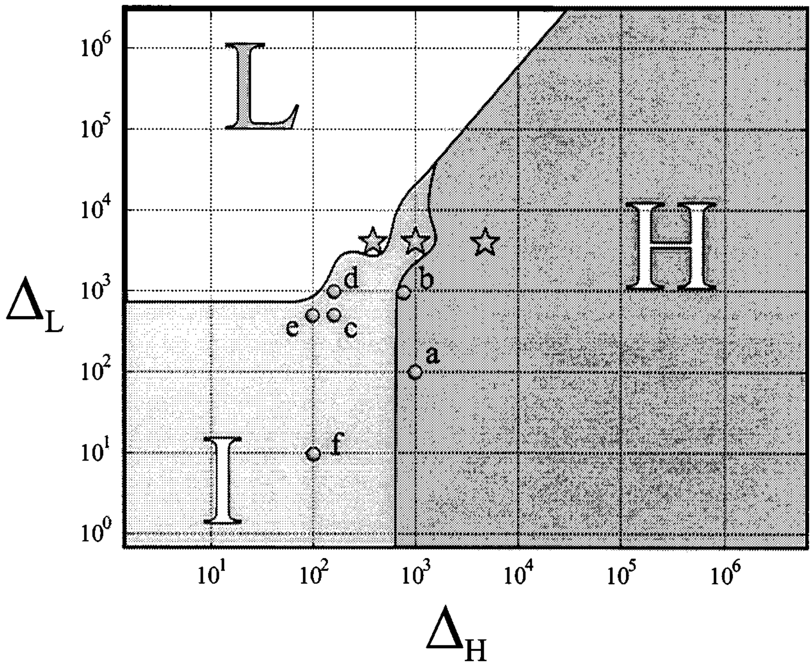

Fig. 6

CCM-BDE 2001. Part I.
I. Zaliapin, V. Keilis-Borok, M. Ghil

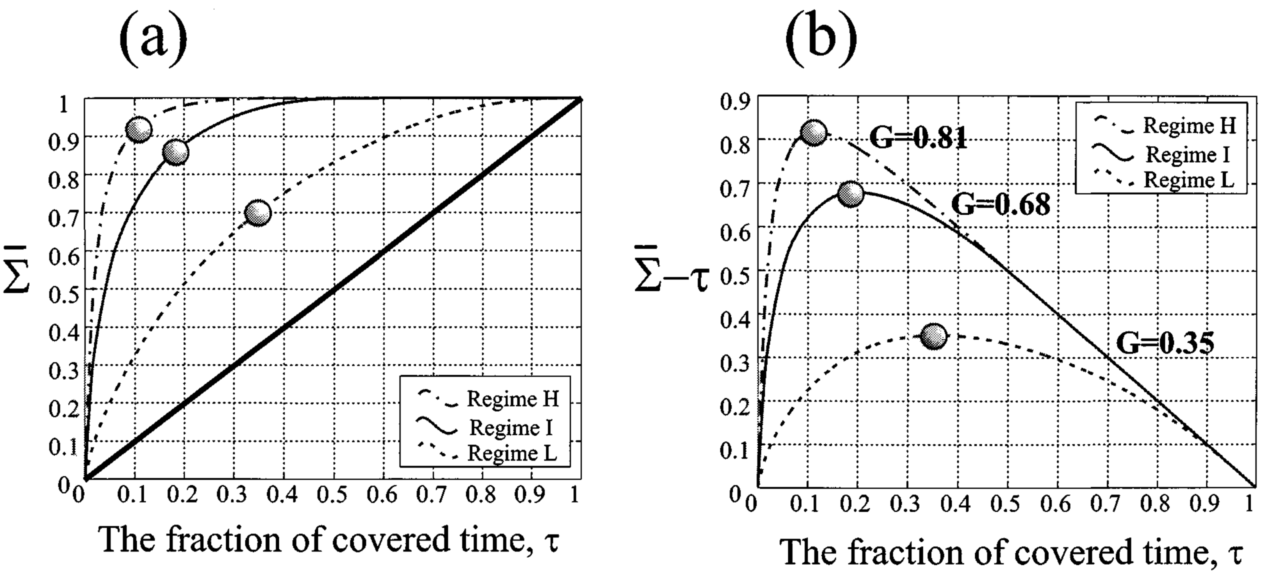
(a)
(b)
Regime H
Regime I
Regime L
G=0.81
G=0.68
G=0.35
The fraction of covered time, τ
The fraction of covered time, τ
$\bar{\Sigma}$
$\bar{\Sigma}-\tau$

Fig. 7

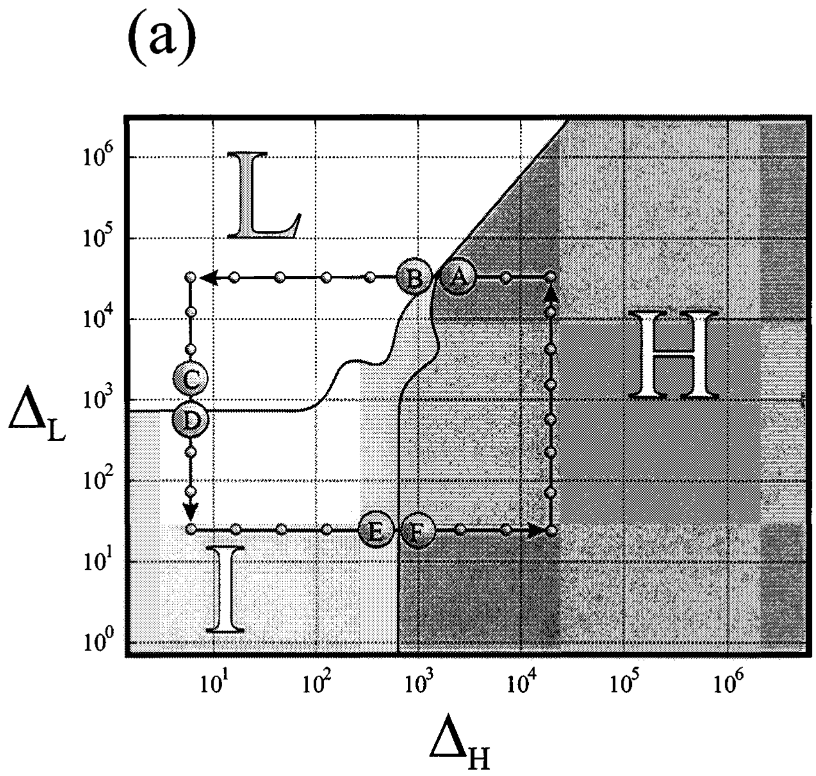

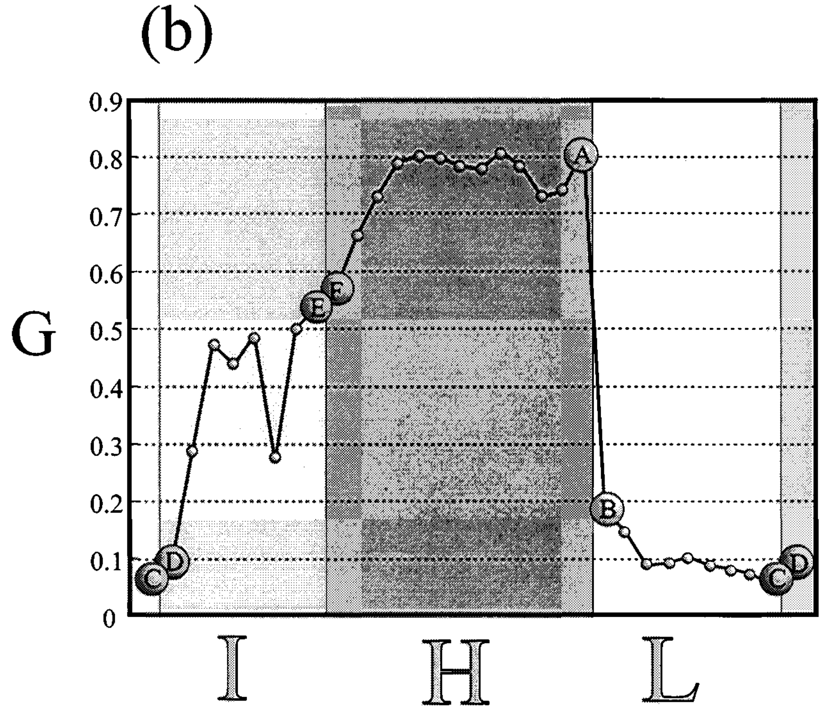

Fig. 8

CCM-BDE 2001. Part I.
I. Zaliapin, V. Keilis-Borok, M. Ghil

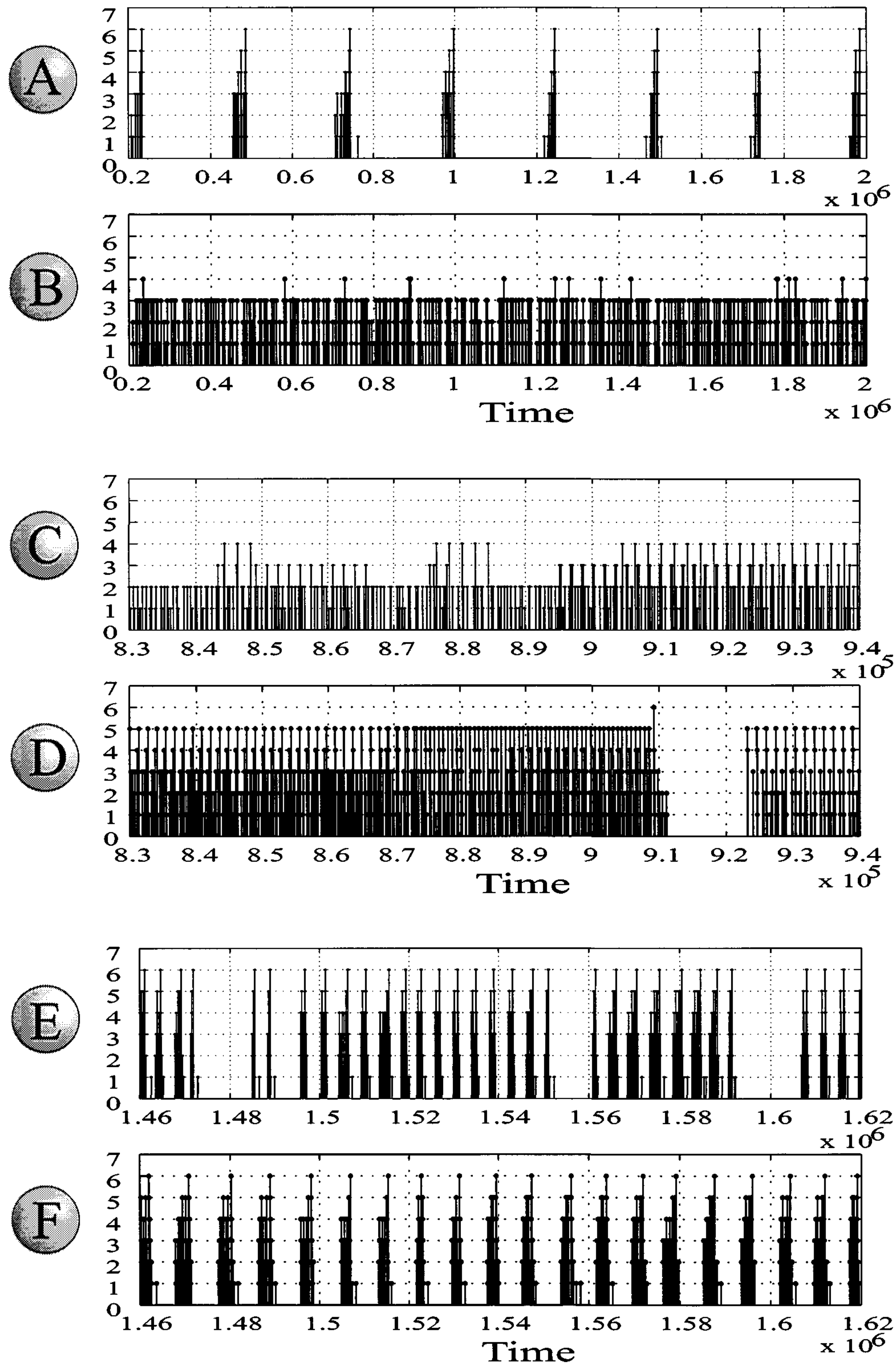

Fig. 9

CCM-BDE 2001. Part I.
I. Zaliapin, V. Keilis-Borok, M. Ghil

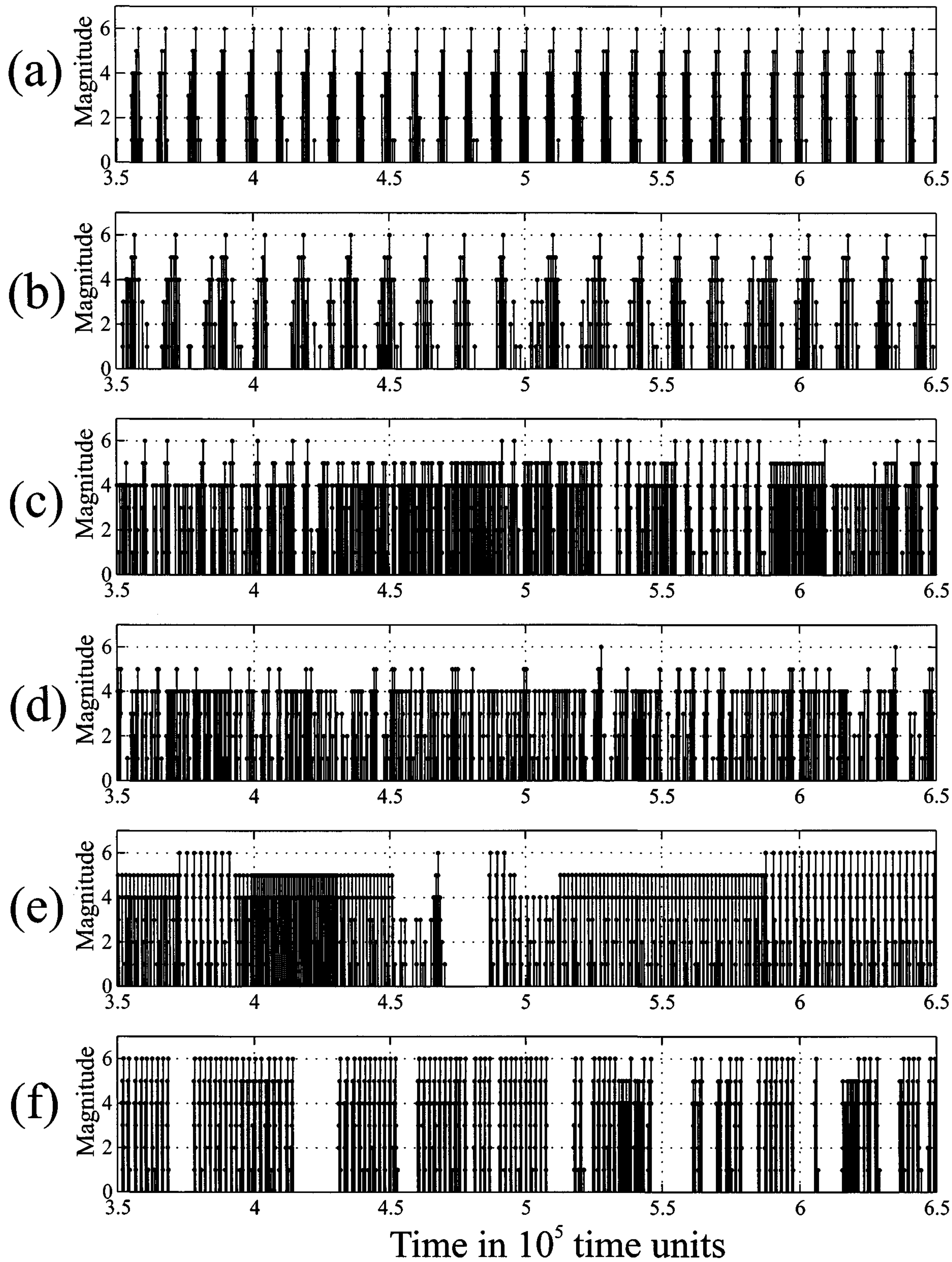

Fig. 10

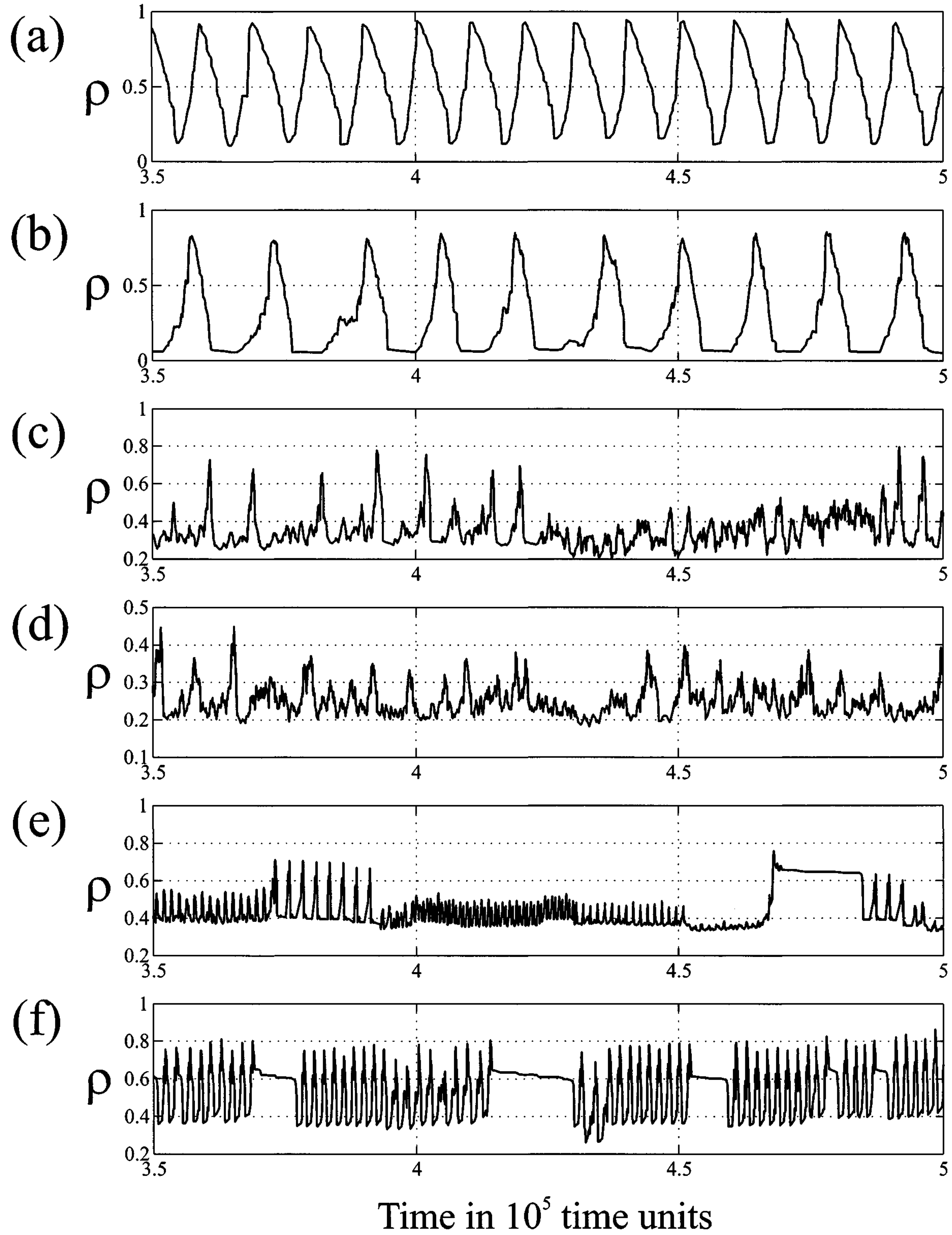

Fig. 11